marine ecology

Marine Ecology. ISSN 0173-9565

ORIGINAL ARTICLE

Swimming speeds of polychaete larvae collected near deep-sea hydrothermal vents

Stace E. Beaulieu[1], R. Thomas Sayre-McCord[1], Susan W. Mills[1], Florence Pradillon[2] & Hiromi Watanabe[3]

1 Woods Hole Oceanographic Institution, Woods Hole, MA, USA
2 Institut français pour l'exploitation de la mer, Plouzané, France
3 Japan Agency for Marine-Earth Science and Technology, Natsushima-cho, Yokosuka, Japan

Keywords
Hydrothermal vent; larval dispersal; Mariana back-arc; swimming behavior.

Correspondence
Stace E. Beaulieu, Biology Department, Mail Stop 34 Woods Hole Oceanographic Institution, Woods Hole, MA 02543 USA.
E-mail: stace@whoi.edu

Accepted: 21 June 2014

doi: 10.1111/maec.12207

Abstract

For benthic fauna endemic to hydrothermal vents, larval dispersal in the plankton is required for maintenance of populations and colonization of new vents. Dispersal distances in the plankton are expected to be influenced by vertical positioning into horizontal currents, and larval survival in the plankton as well as encounter rates for settlement cues may be influenced by swimming speed. Here, we present the first quantitative measurements of swimming speeds of polychaete larvae collected near deep-sea hydrothermal vents. We focused on three polychaete larvae of different morphotypes, with two morphotypes identified genetically to Capitellidae and Spionidae. Mean swimming speeds and helical parameters of the deep-sea polychaete larvae (measured at 1 atm) were similar to values reported for shallow-water polychaete larvae, with mean helical 3D swimming speeds ranging from 0.8–1.4 mm·s^{-1}. To account for swimming that deviated from helical patterns, we developed a new method to reconstruct 3D swimming trajectories, using the 2D track and larval orientation. Speeds were generally faster for downward swimming, with mean vertical displacement speeds ranging from 0.6–0.8 mm·s^{-1} downward as compared with 0.2–0.6 mm·s^{-1} upward. Mean swimming speeds and helical parameters differed among the individuals. Our results are a first step towards constraining a behavioral component in models of larval dispersal between deep-sea hydrothermal vents.

Introduction

Hydrothermal vents are spatially discrete and temporally variable habitats in the deep sea. For benthic species endemic to vents, larval dispersal in the plankton is required for maintenance of populations and colonization of new vents. Larval behavior has the potential to affect dispersal distances and successful settlement at vents. Particle-tracking models to simulate larval dispersal between vents at the East Pacific Rise have indicated that vertical distribution of larvae would impact dispersal distances, due to sheared currents influenced by ridge topography (McGillicuddy *et al.* 2010; Mullineaux *et al.* 2013). For larvae in shallow-water systems, physical–biological modeling of larval dispersal often incorporates information on larval swimming speeds (*e.g.* Guizien *et al.* 2006; North *et al.* 2008; Metaxas & Saunders 2009), and swimming behaviors have been observed to change when a larva senses and responds to settlement cues (*e.g.* Krug & Zimmer 2000; Hadfield & Koehl 2004). However, there is extremely limited quantitative knowledge of the behavior of deep-sea larvae, precluding the incorporation of this factor into models of dispersal.

Here we present the first quantitative measurements of swimming trajectories for polychaete larvae collected near deep-sea hydrothermal vents. Recent papers have reported qualitative information on deep-sea larval swimming behavior at 1 atm (*e.g.* Miyake *et al.* 2010; Reynolds

et al. 2010; Metaxas 2011), but to the best of our knowledge, the only quantitative information is for vent crab megalopae (Epifanio *et al.* 1999) and cold-seep mollusks (Van Gaest 2006; Arellano 2008). Knowledge of the ability of larvae from deep-sea vents to influence their vertical position or react to cues in the water column will contribute to more realistic estimates of larval dispersal than those assuming passive transport. Our results for polychaete larvae at 1 atm are a first step towards constraining a behavioral component in models of larval dispersal between deep-sea hydrothermal vents.

Material and Methods

Study area

Our study was performed in September 2010 on R/V *Yokosuka* Cruise YK10-11. Sampling for these experiments was conducted at 2850-m depth near Snail vent (12°57′ N, 143°37′ E), at 2925-m depth near Urashima vent (12°55′ N, 143°39′ E) and at 3050-m depth near Archaean vent (12°56′ N, 143°38′ E) at the southern Mariana back-arc spreading center.

Collection of larvae

To collect larvae, we deployed large-volume plankton pumps (McLane WTS-LV50, East Falmouth, MA, USA) to sample at 3 or 4 m above the bottom. Each pump sampled for 24 h at 30 $l \cdot min^{-1}$ over a 63-μm mesh, yielding a filtered volume of 41.5 m^3. Upon recovery, pump filters were rinsed with filtered seawater into trays on ice and examined live to sort individual larvae into six-well plates. Many polychaete larvae were alive and active and placed in the dark in a refrigerator at 4 °C.

Video imaging

Swimming behavior was recorded within hours after each pump recovery by video imaging at 1 atm in light. Our experimental chamber was a vertically oriented [4.4 cm (z) × 1 cm (x) × 1 cm (y)], clear, flat-faced cuvette, filled with chilled (4 °C) filtered seawater. To capture video of the front view (*i.e.* xz-plane), we used a high-definition Panasonic HDC-HS60K camcorder, recording at 29.97 frames per second (fps). The lower 3 cm of the cuvette was recorded by the camera with the focal plane in the center, but the entire 1-cm cross-section of the chamber was in the depth of field. Pixel calibration (16.7 μm per pixel) was performed using a grid of 1-mm squares at the center of the chamber. Above the chamber we also mounted a down-looking video camera; however, it did not have fine enough resolution or great enough depth of field to provide useful data in the third (y) dimension. Swimming individuals were introduced gently at the top using a pipette with approximately 10 μl volume, oriented horizontally so as not to impart downward momentum. Although the size of the cuvette was not ideally suited for measurement of movements in three dimensions, it still provided ample space for the larvae to swim in helical patterns. The size of our chamber and the experimental set-up was similar to that used by Guizien *et al.* (2006; excluding infra-red light).

Identification of larvae

After recording each video, we removed each individual from the chamber, measured its length under a compound microscope and assigned it to morphologic group (morphotype). Each individual was saved separately, either frozen or preserved in ethanol. We obtained genetic identifications for a subset of the polychaete larvae *via* barcoding of the mitochondrial cytochrome I oxidase gene (COI). DNA was extracted from whole individual larvae following a protocol by Schizas *et al.* (1997). Sequences were edited and assembled using CodonAligner, and identifications were performed by comparing our sequences with those from publicly available databases (GenBank and BOLD). In GenBank, the BlastX tool was used to search for sequence similarity at the amino acid level, using the codon code for mitochondrial invertebrate DNA. BOLD has a more extensive database for COI, but many sequences are associated with unvalidated taxonomical information and, thus, was used only to confirm and complete GenBank searches.

Video processing

Due to ship motion and vibration, the first step in video processing was stabilization (*i.e.* registration to first frame of video clip), using 'in-house' MATLAB scripts. To track an individual larva and measure the parameters of its 2D projection in a registered video clip, we wrote a MATLAB script, available for download (larval_tracking.m; Supporting Information File S1). The initial position of the larva was selected manually in each video clip. For every fourth frame in the video (*i.e.* ~7.5 fps), the MATLAB tracking function automatically located the larva and, for its 2D projection, output position, length, width, area and planar angle of orientation of the thresholded ellipse. To improve the tracking and measurement of the projected dimensions, variations in each video frame were removed by equalizing lighting, subtracting the average (background) image and thresholding at a low level. We note that thresholding made the projected ellipse slightly larger than the measured larva.

Calculating swimming speeds and helical parameters

Prior to calculating swimming speeds and helical parameters, 2D positions were smoothed with a cubic spline (*e.g.* Menden-Deuer 2010). For each larva's 2D speed in the xz-plane, vertical (v_z) and horizontal (v_x) components of velocity were determined per time step using a three-point centered difference method on the position data. Failure to account for the third dimension in larval swimming trajectories can bias estimates of swimming speeds (*e.g.* Boakes *et al.* 2011; Dur *et al.* 2011). 3D swimming speeds were estimated in two ways. First, we applied an equation for helical swimming to the 2D observations to calculate the 3D speed along the helix (v_{3helix}):

$$v_{3helix} = \sqrt{{v_{axis}}^2 + (2\pi fA)^2} \quad (1)$$

where v_{axis} is the speed along the axis of the helix, f is the turn frequency of the helix and A is the amplitude of the helix (*e.g.* Svensen & Kiørboe 2000). To estimate helical swimming speeds and parameters, the larval trajectory was split into half pitches using the intersections of the 2D trajectory with the 2D axis of travel (*sensu* Chan & Grünbaum 2010). We smoothed the 2D axis of travel with a cubic spline of the xz-positions at the start, middle and end of each full helical pitch. Speed along the 2D axis of travel, turn frequency and amplitude were determined per half pitch, with amplitude as the maximum distance between the 2D trajectory and the 2D axis of travel, pitch determined from displacements along the 2D axis of travel and axis speed as pitch multiplied by turn frequency (note: this would be 1D vertical displacement speed if there was perfect vertical orientation of the helix). Most other studies measuring only two dimensions of larval swimming trajectories have estimated the third dimension based on isotropy or assumed swimming behavior (*e.g.* Svensen & Kiørboe 2000; Chan & Grünbaum 2010; Gurarie *et al.* 2011).

Second, we used a new method, described here, that requires only 2D imaging data yet makes no assumptions about the nature of the swimming trajectory being measured. We propose this method for organisms with body shapes that can be approximated as elongated ellipsoids. Assuming that the organism does not change shape and is swimming at a constant angle with respect to its body axis, the third dimension of motion can be reconstructed trigonometrically using the two recorded dimensions and the orientation of the organism with respect to the video plane. The orientation of the organism is determined by comparing the dimensions of the 2D projection of the organism onto the video plane with known 3D dimensions of the organism (if physical measurements of the specimen are lacking, the approximation can be made using the projected ellipse with maximum aspect ratio). We present the full set of equations for this reconstruction method in Appendix 1.

To apply the trigonometric method to our imaged deep-sea polychaete larvae, we approximated each individual as a prolate spheroid (ellipsoid with semi-axis lengths a > b = c). Thus, rotation of the larva is not considered and only the length of the 2D projection (L) is required to find the angle of inclination (γ) into/out of the plane using equations (2) and (3) [reduced from equations (13) and (14) in Appendix 1]:

$$\phi_0 = \tan^{-1}\left(\frac{-b}{a}\tan\gamma\right) \quad (2)$$

$$L(\gamma) = 2a\cos\gamma\cos\phi_0 - 2b\sin\gamma\sin\phi_0 \quad (3)$$

where φ_0 is a temporary angle for calculation. Equation (3) may be solved numerically to give a one-to-one relationship between L and γ. The approximation to prolate spheroid allows for the use of width as a normalization factor, to remove effects of depth of field or residual lighting effects. The 3D speed (v_{3recon}) is found trigonometrically using the measured 2D speed (S_2) in the xz-plane and the angle of inclination found above:

$$v_{3recon} = \frac{S_2}{\cos\gamma} \quad (4)$$

Using the 3D speed (v_{3recon}) and the measured 2D speed (S_2), the horizontal speed in the reconstructed direction (y) can be found for every point in time:

$$v_y = \sqrt{{v_{3recon}}^2 - {S_2}^2} \quad (5)$$

and thus, each y-position. Our MATLAB script for the 3D reconstruction method for a prolate spheroid is available for download (reconstruct_3D.m; File S2). An empirical test using 3D video recordings from two orthogonal cameras validated this 3D trajectory reconstruction method for a similar-sized polychaete larva from shallow water (File S3). Curvature and torsion of each larva's 3D reconstructed trajectory were found using the numerical techniques described by Crenshaw *et al.* (2000; with a modification to their equation (20), applying the arccosine to the entire first term in parentheses).

In addition to calculating swimming speeds and helical parameters for each trajectory as a whole, we also estimated upward- *versus* downward-oriented swimming speeds separately. Reconstructed 3D speeds were assigned as upward- or downward-oriented based on the vertical displacement per time step (z-component of velocity). Analyses were restricted to video segments >3 s (*e.g.* Menden-Deuer

2010) with tracked positions >2 mm above the bottom of the chamber to avoid a boundary (wall) effect. Sinking speeds for those larvae that exhibited no behavior in the experimental chamber are reported as a single value for vertical displacement speed.

To quantify temporal variation along an individual track, swimming speeds and helical parameters are reported as means with standard deviation. However, we must stress that these are values determined per time step for single trajectories. Aside from two runs of one individual, there was no replication of our experiments. A usual practice in reporting larval swimming behavior is to acquire a single value per trajectory for swimming speeds and helical parameters. To acquire replicates, *e.g.* of a larval type in an experimental treatment, multiple trajectories are recorded (*e.g.* Chan & Grünbaum 2010; Hansen *et al.* 2010). Thus, a formal statistical test to compare mean values can not be performed on our data. Furthermore, and similar to Menden-Deuer (2010), 2D speed data were autocorrelated over the measured path durations; thus, there is no de-correlation time by which to segment data for exploratory statistics. Helical 3D speed (v_{3helix}), axis speed (v_{axis}), amplitude, pitch and frequency were determined per half pitch; thus, the reported values are weighted for the duration of each half pitch. Mean values for curvature and absolute value of torsion are based on slightly fewer numbers of time steps due to removal of outliers at >3 standard deviations.

Results

Helical speeds and parameters for swimming trajectories

Three individuals of different morphotypes were actively swimming upon introduction to the vertical chamber. One was identified genetically to the family Capitellidae, and the second was of morphotype chaetosphaerid (others of this morphotype were identified genetically to Spionidae). The third was of morphotype '4-ciliary band metatrochophore', which has not yet been genetically identified (Fig. 1). From here on, these individuals are referred to as the capitellid, the chaetosphaerid and the metatrochophore. The larvae generally swam in a helical pattern, although the pattern varied especially for the chaetosphaerid and capitellid (Fig. 2). Entire trajectories could be tracked for the two runs with the capitellid, while the chaetosphaerid and the metatrochophore were tracked in 18 and 12 separate video segments (with analyses restricted to 12 and 2), respectively. Mean helical 3D speeds (v_{3helix}) appeared to differ among the three individuals, ranging from 0.8 $mm{\cdot}s^{-1}$ for the smaller metatrochophore to 1.4 $mm{\cdot}s^{-1}$ for the larger chaetosphaerid (Table 1). The capitellid, intermediate in size, was intermediate in v_{3helix} (similar in its two trials). Mean helical axis speeds (v_{axis}) ranged only from 0.5–0.7 $mm{\cdot}s^{-1}$ (Table 1); however, this speed along a 2D helical axis may underestimate the true 3D helical axis speed, especially for the chaetosphaerid, which utilized much of the chamber volume (Fig. 2C). Speeds for the metatrochophore may be slight underestimates due to the potential for wall effects (Fig. 2D).

The individuals also appeared to differ in turn frequency and other helical parameters. The capitellid was intermediate in turn frequency, ~0.4 s^{-1} in both trials, while the chaetosphaerid turned at just more than half that rate and the metatrochophore at about a 50% faster rate (Table 2). The capitellid also was intermediate in other measured helical parameters, with the exception of curvature (Table 2). Values for helical parameters matched well in the two trials of the capitellid (Table 2), with the first run more variable in curvature (Fig. 2A).

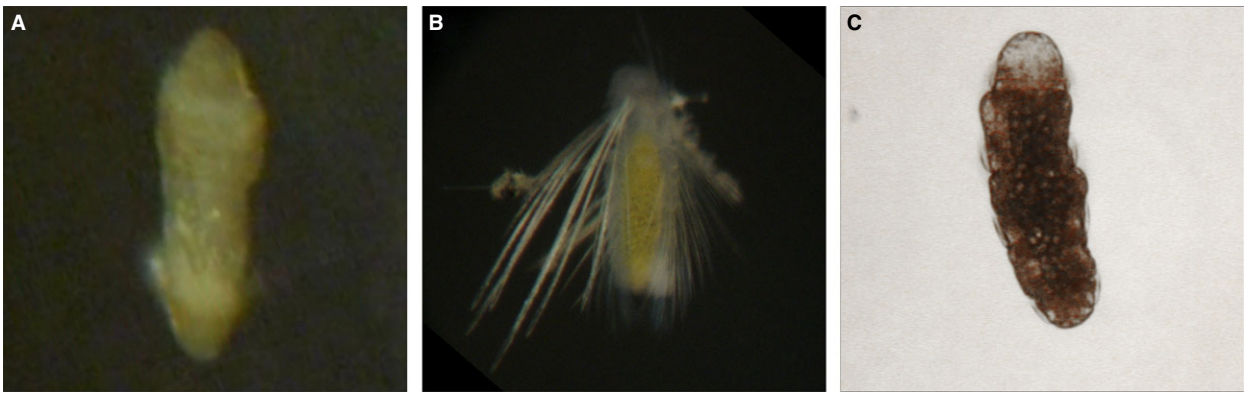

Fig. 1. Live photographs of deep-sea polychaete larvae (or larval morphotypes) for which swimming speeds are presented in Table 1. (A) Capitellid used in experiment, genetically identified to family Capitellidae, length 340 μm. (B) Chaetosphaerid, genetically identified to family Spionidae, length 585 μm (the chaetosphaerid in the experiment was not genetically identified). (C) '4-ciliary band metatrochophore', length 395 μm (morphotype not genetically identified).

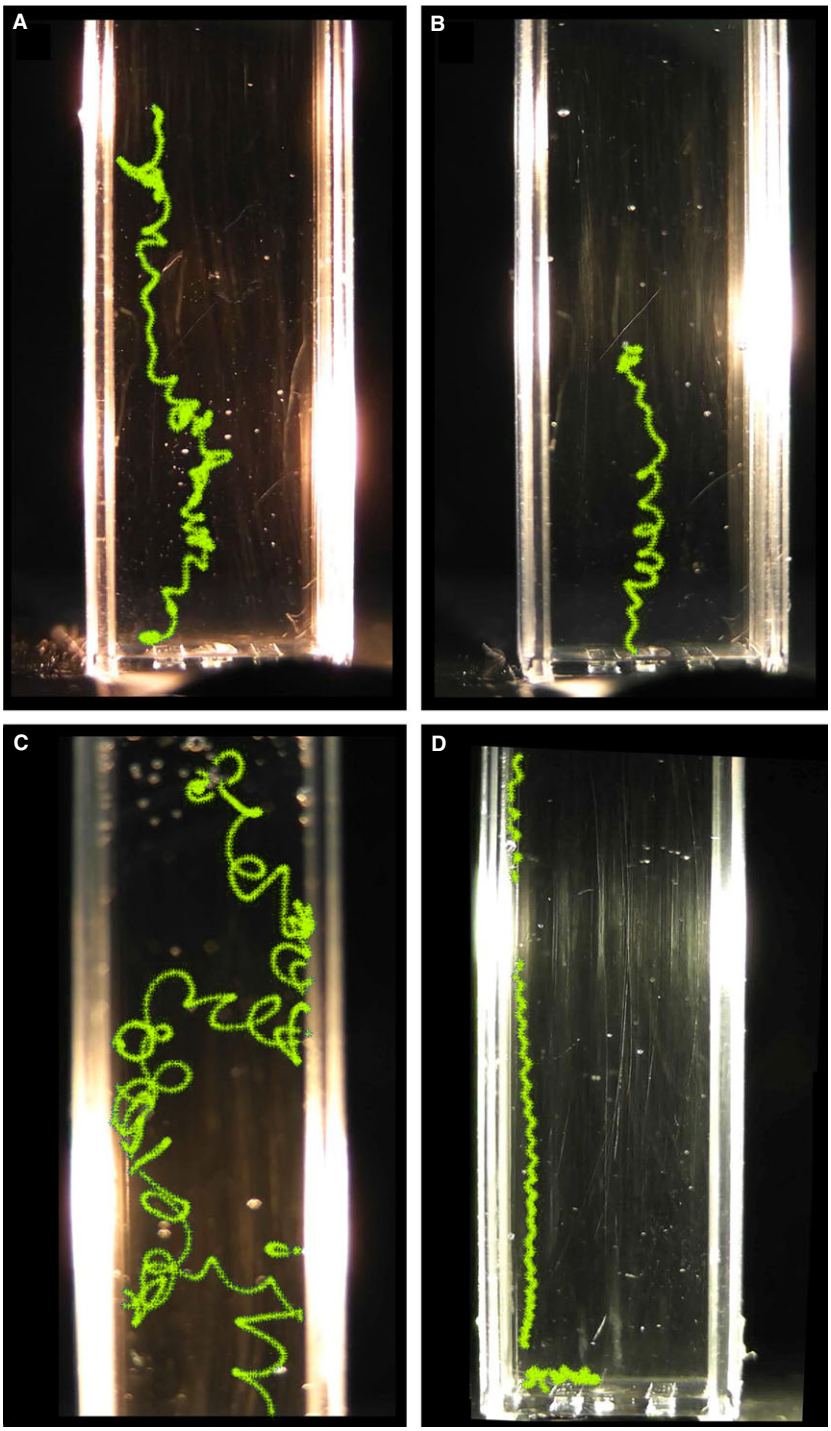

Fig. 2. Larval swimming trajectories with positions tracked in 2D, super-imposed on video frame grab. Field of view is the lower ~3 cm of the experimental chamber (1-cm width). Each trajectory starts at the top and ends at the bottom. Gaps occur in (C) and (D) where the larva was not tracked. (A) Capitellid larva first trial. (B) Capitellid larva second trial. (C) Chaetosphaerid (likely spionid) larva. (D) '4 ciliary band metatrochophore'.

Differences among individuals in amplitude (and curvature) and pitch (and torsion) are evident visually (Fig. 2). The metatrochophore exhibited the least mean helical amplitude (0.1 mm, about half its body length), as compared with the chaetosphaerid, which was greatest in amplitude (0.7 mm, about twice its body length) and least in curvature (Table 2). Similarly, the metatrochophore was least in helical pitch (0.8 mm, about three body lengths) with the greatest torsion (tightest half-pitch crossings), and the chaetosphaerid was greatest in pitch (2.8 mm, about eight body lengths) with the least torsion (Table 2).

Table 1. Helical swimming speeds (weighted mean ± SD) for each larval trajectory. Axis speed (v_{axis}) is speed along 2D helical axis, input to equation (1) to obtain 3D speed along the helix (v_{3helix}). Time is the total time of tracked larval positions for the trajectory, excluding the positions before the first and after the last half-pitch crossings. n is the number of half pitches used in calculations. The mean reconstructed 3D speed (v_{3recon}) for the entire trajectory is shown for comparison. Body length was determined under a microscope and aspect ratio was determined from thresholded pixels in the video.

Larval type	Body length (μm) (and aspect ratio)	v_{axis} axis speed (mm · s^{-1})	v_{3helix} helical 3D speed (mm · s^{-1})	Time (s)	n half pitch	v_{3recon} reconstructed 3D speed (mm · s^{-1})
Capitellid (two trials with same individual)	340 (2.4)	0.5 ± 0.2	1.1 ± 0.3	89.2	80	1.2 ± 0.2
		0.5 ± 0.3	1.2 ± 0.3	31.1	27	1.2 ± 0.2
Chaetosphaerid (likely spionid)	350 (1.5)	0.7 ± 0.4	1.4 ± 0.4	91.6	49	1.7 ± 0.7
'4 ciliary band metatrochophore'	260 (2.4)	0.6 ± 0.2	0.8 ± 0.2	28.2	43	0.7 ± 0.2

Table 2. Helical parameters (mean±SD), with amplitude, pitch and turn frequency as weighted means. Helical amplitude and turn frequency are input to equation (1) to obtain 3D speed along the helix in Table 1 (time and number of half pitches as in Table 1).

Larval type	Helical amplitude (mm)	Helical pitch (mm)	Turn frequency (per second)	Curvature (radian · mm^{-1})	Torsion (radian · mm^{-1})
Capitellid (two trials with same individual)	0.4 ± 0.2	1.3 ± 0.8	0.4 ± 0.2	2.8 ± 1.9	2.0 ± 1.4
	0.4 ± 0.1	1.3 ± 0.8	0.4 ± 0.1	2.2 ± 1.0	1.7 ± 1.2
Chaetosphaerid (likely spionid)	0.7 ± 0.3	2.8 ± 1.4	0.3 ± 0.1	0.9 ± 0.6	1.4 ± 1.0
'4 ciliary band metatrochophore'	0.1 ± 0.0	0.8 ± 0.2	0.8 ± 0.1	2.1 ± 0.8	7.3 ± 3.1

Reconstructed 3D swimming trajectories

Reconstructed 3D speeds (v_{3recon}) for the trajectories were similar to helical 3D speeds (v_{3helix}) (Table 1). The reconstructed 3D trajectory for the first trial of the capitellid is shown in Fig. 3A. Although the mean v_{3recon} for the chaetosphaerid was slightly greater than v_{3helix}, this would be expected if its v_{axis} was an underestimate (as suggested above), and there was considerable temporal variability in the estimated 3D speed along its track (greatest SD; Table 1). Mean 2D speeds, used in equation (5), underestimated the mean reconstructed 3D speeds by 8% for the metatrochophore, 27–32% for the capitellid and 32% for the chaetosphaerid.

Upward *versus* downward-oriented swimming speeds

Speeds were generally faster for the downward portions of the swimming trajectories (Table 3). Downward displacement (1D) speeds were greater than upward for the chaetosphaerid and both runs of the capitellid. Downward reconstructed 3D speeds were greater than upward for the chaetosphaerid and the second run of the capitellid (which also had a lower mean value for upward vertical displacement speed). Mean vertical displacement speeds (v_z) differed among the individuals, ranging from 0.2–0.6 mm·s^{-1} upward and 0.6–0.8 mm·s^{-1} downward. Although the metatrochophore exhibited upward swimming after contacting the bottom, analyses were not performed due to the brevity of the clips and the expected wall effects (Fig. 2D). Mean 3D reconstructed speeds (v_{3recon}) also differed among the individuals, ranging from 1.0–1.5 mm·s^{-1} upward and 0.7–1.8 mm·s^{-1} downward. Seven other individuals, classified to four different morphotypes (including the two morphotypes genetically identified to Capitellidae and Spionidae), dropped without apparent behavior in the experimental chamber. Their sinking speeds ranged widely (0.4–1.1 mm·s^{-1}) and did not correlate to size within a morphotype (Table 4).

Discussion

With the caveats explained below, the 3D swimming speeds of the deep-sea polychaete larvae, in the order of 1 mm·s^{-1}, are on the lower end but well within the range of speeds reported for shallow-water polychaete larvae (Chia *et al.* 1984). We might expect speeds at the lower end because the experiments were conducted at low temperature, which would lower metabolic rate and increase viscosity of the fluid (*e.g.* Young 1995). The deep-sea capitellid larva swam more slowly than shallow capitellid larvae that had mean horizontal swimming speeds of 1.6–3.3 mm·s^{-1} (Butman *et al.* 1988). However, the shallow capitellid larvae swam more slowly in light, at speeds consistent with the mean speed of the deep-sea larva. The deep-sea chaetosphaerid (likely spionid) larva swam faster and with greater helical amplitude than reported for

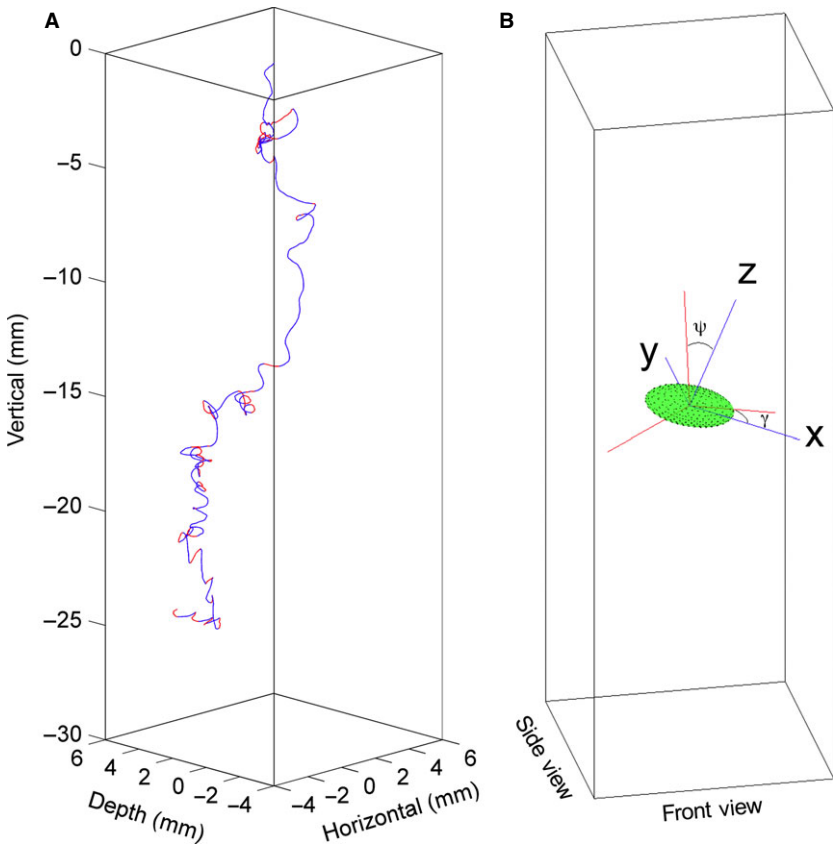

Fig. 3. (A) Reconstructed 3D trajectory for capitellid larva in Fig. 2A (first trial in Tables 1–3). Blue indicates downward- and red indicates upward-oriented swimming. (B) Diagram of angles used in Appendix 1. Blue lines show x-, y- and z-axes in body fixed frame used for calculation in Appendix 1, and red lines show the internal axes of the ellipsoid after rotation. Prior to any rotation the calculation axes and internal axes are the same.

Table 3. Vertical displacement (v_z) and reconstructed 3D (v_{3recon}) swimming speeds (mean±SD) for the upward *versus* downward-oriented swimming. Time up or down is the total time that the larva had a positive or negative vertical velocity, respectively. For the '4 ciliary band metatrochophore', reconstructed 3D speed is the same as in Table 1 because the individual only moved downward in the clips analysed.

Larval type	v_z vertical displacement speed (mm · s^{-1}) up/down	v_{3recon} reconstructed 3D speed (mm · s^{-1}) up/down	Time (s) up/down
Capitellid (two trials with same individual)	0.4 ± 0.2/0.6 ± 0.4	1.1 ± 0.2/1.2 ± 0.2	28.6/61.4
	0.2 ± 0.2/0.7 ± 0.3	1.0 ± 0.2/1.3 ± 0.2	7.2/24.8
Chaetosphaerid (likely spionid)	0.6 ± 0.4/0.8 ± 0.5	1.5 ± 0.5/1.8 ± 0.7	48.7[a]/65.3
'4 ciliary band metatrochophore'	–/0.6 ± 0.2	–/0.7 ± 0.2	–/29.6

[a]The 3D reconstruction failed for 1 s in an upward swimming portion of one of the 12 clips.

larvae of an estuarine spionid (Hansen *et al.* 2010). In general, the helical amplitudes of the deep-sea larvae (Table 2) were consistent with the range of values reported for shallow-water polychaete larvae (*e.g.* Bolton & Havenhand 1997; Guizien *et al.* 2006; Hansen *et al.* 2010). As found by Hansen *et al.* (2010), the larvae swam downwards faster than upwards, likely influenced by gravity as all of the non-swimming individuals appeared to be negatively buoyant. Our measurements for sinking without apparent behavior were consistent with other more accurate measurements of settling velocities for shallow-water polychaete larvae, *e.g.* ~0.8 mm·s^{-1} for *Owenia fusiformis* (reviewed by Guizien *et al.* 2006) and 0.8–1.0 mm·s^{-1} for *Capitella* sp. (Butman *et al.* 1988). Our results for 3D swimming speeds and helical trajectories will be important for modeling small-scale physical–biological interactions such as encounter rates (*e.g.* Visser & Kiørboe 2006; Menden-Deuer 2010) or detection of

Table 4. 'Sinking' speeds (*i.e.* dropping without apparent behavior).

Larval type	Body length (μm)	Vertical drop speed (mm · s^{-1})
Chaetosphaerid, genetic ID Spionidae	355	0.4
Nectochaete[a]	300	0.4
Capitellid morphotype[b]	790	0.5
Chaetosphaerid[c]	200	0.6
Capitellid morphotype[b]	595	0.6
Complex nectochaete[d]	430	0.8
Chaetosphaerid[c]	350	1.1

[a]Other similar-looking specimens genetic ID Alvinellidae.
[b]Other similar-looking specimens genetic ID Capitellidae.
[c]Other similar-looking specimens genetic ID Spionidae.
[d]Other similar-looking specimens genetic ID Hesionidae.

chemical gradients (*e.g.* Boakes *et al.* 2011), *e.g.* for settlement cues associated with hydrothermal plumes.

Our results for vertical displacement speeds (v_z) are a first step towards constraining a behavioral component in models of larval dispersal between deep-sea hydrothermal vents. An upward displacement speed of 0.5 mm·s^{-1} corresponds to 43.2 m·day^{-1}, or 5 days for a larva to swim up to the height of a typical hydrothermal plume (~200 m above bottom). A recent particle tracking model for the East Pacific Rise (EPR) simulated 'balloonist' larvae at 225 m above bottom (McGillicuddy *et al.* 2010). Along-ridge transport in this model was very sensitive to vertical position of tracked particles, with a reduction in maximal transport distances for balloonist larvae compared with simulated larvae dispersing near-bottom in faster ridge-flank currents. When considering specifically the axial trough of the EPR, Mullineaux *et al.* (2013) suggested downward-moving behavior (swimming or sinking) as a means of 'behaviorally mediated retention of vent larvae' for reducing transport off-axis. In other regions in which vents are distributed at very different water depths, for example in the Mariana arc/back-arc system, upward- and downward-oriented swimming would be crucial for physical connectivity as the magnitude of vertical displacement speeds greatly exceeds cross-isopycnal (diapycnal) velocity in the deep sea. Models of larval dispersal are recommended for the design of marine reserves for deep-sea vents that may become the target for polymetallic sulfide mining (Van Dover *et al.* 2011). The three individuals reported in this study were collected near hydrothermal vents, but have not yet been matched to species endemic to the vents. Although not yet reported for hydrothermal vents in the Mariana region, species in the families Capitellidae and Spionidae are found at deep-sea hydrothermal vents in other regions (*e.g.* Hourdez *et al.* 2006; Levin *et al.* 2009).

We would like to identify several caveats to be considered in interpreting these first direct measurements of swimming speeds of deep-sea polychaete larvae, starting with issues involved in studying behavior *ex situ*. First, as these larvae would be adapted to high pressure, it would be preferable to conduct the experiments not at 1 atm but in a pressure chamber at ~300 atm. It is unknown whether the lower pressure in our experiments would alter behavior or metabolic rate and affect swimming speeds or paths. Second, it would be preferable to measure swimming speeds of these larvae in the dark. Larvae of most polychaete taxa have eyes, and light may be a stressor or may alter directional behavior. Shallow-water polychaete larvae can behave differently in light *versus* infra-red conditions (*e.g.* Butman *et al.* 1988; Guizien *et al.* 2006). However, the use of infra-red light might actually be a complication with deep-sea vent larvae due to potential response to infra-red light as a settlement cue (Van Dover *et al.* 1996). Other stressors during sampling and experimentation could include the physical stress of being collected onto a filter or into a pipette. We minimized temperature effects (and consequent viscosity effects) by conducting the experiments with cold filtered seawater (note: elevated temperatures would only be experienced by vent larvae in the extreme proximity of a vent, otherwise they are exposed to ambient temperatures of 2 °C in the deep Mariana Trough). However, as we used surface-derived seawater we could improve on this by collecting the seawater at depth to better approximate the dissolved water chemistry.

Additional caveats to be considered in interpreting these measurements of swimming speeds include the experimental chamber itself and the methods used to estimate 3D speed from 2D tracks. Similar to Guizien *et al.* (2006), larval trajectories were constrained by the size of the chamber. The larvae were small enough that hydrodynamic surface effects (wall effects) would be <5% near the center of the chamber (*i.e.* >~4 mm from the sides and bottom, or >20 times the equivalent spherical diameter; Drescher *et al.* 2009). We recommend controlling background convective fluid motion by conducting future experiments in a cold room or by using a water bath (*e.g.* Drescher *et al.* 2009) and controlling ship motion by using an anti-vibration table. We developed a new 3D reconstruction method for 2D tracks to account for swimming that deviated from helical patterns; however, the assumption that the organism does not change shape may not hold for the chaetosphaerid because its chaetae may flare out or be pulled in close to its body, thus affecting the thresholded size of the 2D projection. To measure true 3D speed, all three dimensions must be recorded, either with a two-camera set-up (*e.g.* Dur *et al.* 2011) or with a mirror system (*e.g.* Hansen *et al.* 2010).

A third set of caveats to be considered in interpreting these measurements of swimming speeds involves the lack of replication in our study. Our results are specific to three individuals, and the lack of replication precludes determination of whether the differences in swimming speeds and helical parameters are size-specific or species-specific. Size (and life-history stage) are known factors that can affect swimming speeds within a species. For example, Hansen *et al.* (2010) reported a positive correlation between body length and downward swimming speeds in polychaete larvae of a spionid species. We recommend that future experiments employ multiple individuals per morphotype to determine variability within a morphotype, so that differences between morphotypes may be determined with tests of statistical significance.

We note that results from the experiments presented here offer motivation for further studies. For example, our experiments were conducted in the absence of settlement cues. Now we have a baseline for helical patterns at 1 atm – will we see different swimming patterns if a chemical cue is added to the experimental chamber? Swimming trajectories and/or helical parameters might change in response to a chemical cue (*e.g.* Krug & Zimmer 2000; Hadfield & Koehl 2004; Boakes *et al.* 2011). In addition, our trigonometric method for 3D reconstruction of larval swimming trajectories warrants further validation. Other applications of this method include working with legacy data recorded with a single camera (*e.g.* Visser & Kiørboe 2006), or using experimental pressure vessels with a single viewing window (*e.g.* Brooke & Young 2009). We are encouraged to conduct future experiments with pressure vessels to approximate *in situ* conditions, using the 3D reconstruction method if the viewing window(s) are too restricted for orthogonal cameras. With additional software development to track multiple individuals in the same volume, we could increase our sample size and better understand the variability within a morphotype, or species. Species-specific swimming speeds may be important for dispersal models that target particular species for conservation in the future.

Acknowledgements

We thank Chief Scientist S. Kojima and the Captain and crew of R/V *Yokosuka* Cruise YK10-11. We thank T. Silva for video conversion. For the empirical test of the 3D reconstruction method, we thank K. Katija Young for video imaging and B. Pernet and S. Irvine for aid in morphologic identification of the larva. We thank H. Jiang, L. Mullineaux, J. Wheeler, two anonymous reviewers and editors A. Metaxas and C. Young for improvements to the manuscript. This project was supported by NSF OCE-1028862 and OISE-1157556 to S.E. Beaulieu, a WHOI Summer Student Fellowship to R.T. Sayre-McCord, TAIGA project support to H. Watanabe and F. Pradillon, and Canon Foundation support to H. Watanabe.

References

Arellano S.M. (2008) Embryology, larval ecology, and recruitment of "*Bathymodiolus*" *childressi*, a cold-seep mussel from the Gulf of Mexico. Ph.D. Thesis, University of Oregon.

Boakes D., Codling E., Thorn G., Steinke M. (2011) Analysis and modeling of swimming behavior in *Oxyrrhis marina*. *Journal of Plankton Research*, **33**, 641–649.

Bolton T.F., Havenhand J.N. (1997) Physiological versus viscosity-induced effects of water temperature on the swimming and sinking velocity of larvae of the serpulid polychaete *Galeoloria caespitosa*. *Marine Ecology Progress Series*, **159**, 209–218.

Brooke S.D., Young C.M. (2009) Where do the embryos of *Riftia pachyptila* develop? Pressure tolerances, temperature tolerances, and buoyancy during prolonged embryonic dispersal. *Deep-Sea Research II*, **56**, 1599–1606.

Butman C.A., Grassle J.P., Buskey E.J. (1988) Horizontal swimming and gravitational sinking of *Capitella* sp. I (Annelida: Polychaeta) larvae: implications for settlement. *Ophelia*, **29**, 43–57.

Chan K.Y.K., Grünbaum D. (2010) Temperature and diet modified swimming behaviors of larval sand dollar. *Marine Ecology Progress Series*, **415**, 49–59.

Chia F.S., Buckland-Nicks J., Young C.M. (1984) Locomotion of marine invertebrate larvae: a review. *Canadian Journal of Zoology*, **62**, 1205–1222.

Crenshaw H.C., Ciampaglio C.N., McHenry M.J. (2000) Analysis of the three-dimensional trajectories of organisms: estimates of velocity, curvature, and torsion from positional information. *Journal of Experimental Biology*, **203**, 961–982.

Drescher K., Leptos K.C., Goldstein R.E. (2009) How to track protists in three dimensions. *Review of Scientific Instruments*, **80**, 014301.

Dur G., Souissi S., Schmitt F., Michalec F.-G., Mahjoub M.-S., Hwang J.-S. (2011) Effects of animal density, volume, and the use of 2D/3D recording on behavioral studies of copepods. *Hydrobiologia*, **666**, 197–214.

Epifanio C.E., Perovich G., Dittel A.I., Cary S.C. (1999) Development and behavior of megalopa larvae and juveniles of the hydrothermal vent crab *Bythograea thermydron*. *Marine Ecology Progress Series*, **185**, 147–154.

Guizien K., Brochier T., Duchene J.-C., Koh B.-S., Marsaleix P. (2006) Dispersal of *Owenia fusiformis* larvae by wind-driven currents: turbulence, swimming behaviour and mortality in a three-dimensional stochastic model. *Marine Ecology Progress Series*, **311**, 47–66.

Gurarie E., Grünbaum D., Nishizaki M.T. (2011) Estimating 3D movements from 2D observations using a continuous model of helical swimming. *Bulletin of Mathematical Biology*, **73**, 1358–1377.

Hadfield M.G., Koehl M.A.R. (2004) Rapid behavioral responses of an invertebrate larva to dissolved settlement cue. *Biological Bulletin*, **207**, 28–43.

Hansen B.W., Jakobsen H.H., Andersen A., Almeda R., Pedersen T.M., Christensen A.M., Nilsson B. (2010) Swimming behavior and prey retention of the polychaete larvae *Polydora ciliata* (Johnston). *Journal of Experimental Biology*, **213**, 3237–3246.

Hourdez S., Desbruyères D., Laubier L. (2006) *Malacoceros samurai*, a new species of Spionidae (Annelida: Polychaeta) from hydrothermal vent chimney walls on the south East Pacific Rise. *Proceedings of the Biological Society of Washington*, **119**, 592–599.

Krug P.J., Zimmer R.K. (2000) Developmental dimorphism and expression of chemosensory-mediated behavior: habitat selection by a specialist marine herbivore. *Journal of Experimental Biology*, **203**, 1741–1754.

Levin L.A., Mendoza G.F., Konotchick T., Lee R. (2009) Macrobenthos community structure and trophic relationships within active and inactive Pacific hydrothermal sediments. *Deep-Sea Research II*, **56**, 1632–1648.

McGillicuddy D.J. Jr, Lavelle J.W., Thurnherr A.M., Kosnyrev V.K., Mullineaux L.S. (2010) Larval dispersion along an axially symmetric mid-ocean ridge. *Deep-Sea Research II*, **57**, 880–892.

Menden-Deuer S. (2010) Inherent high correlation of individual motility enhances population dispersal in a heterotrophic, planktonic protist. *PLoS Computational Biology*, **6**, e1000942.

Metaxas A. (2011) Spatial patterns of larval abundance at hydrothermal vents on seamounts: evidence for recruitment limitation. *Marine Ecology Progress Series*, **437**, 103–117.

Metaxas A., Saunders M. (2009) Quantifying the "bio-" components in biophysical models of larval transport in marine benthic invertebrates: advances and pitfalls. *Biological Bulletin*, **216**, 257–272.

Miyake H., Kitada M., Itoh T., Nemoto S., Okuyama Y., Watanabe H., Tsuchida S., Inoue K., Kado R., Ikeda S., Nakamura K., Omata T. (2010) Larvae of deep-sea chemosynthetic ecosystem animals in captivity. *Cahiers de Biologie Marine*, **51**, 441–450.

Mullineaux L.S., McGillicuddy D.J. Jr, Mills S.W., Kosnyrev V.K., Thurnherr A.M., Ledwell J.R., Lavelle J.W. (2013) Active positioning of vent larvae at a mid-ocean ridge. *Deep-Sea Research II*, **92**, 46–57.

North E.W., Schlag Z., Hood R.R., Li M., Zhong L., Gross T., Kennedy V.S. (2008) Vertical swimming behavior influences the dispersal of simulated oyster larvae in a coupled particle-tracking and hydrodynamic model of Chesapeake Bay. *Marine Ecology Progress Series*, **359**, 99–115.

Reynolds K.C., Watanabe H., Strong E.E., Sasaki T., Uematsu K., Miyake H., Kojima S., Suzuki Y., Fujikura K., Kim S. (2010) New molluscan larval form: brooding and development in a hydrothermal vent gastropod, *Ifremeria nautilei* (Provannidae). *Biological Bulletin*, **219**, 7–11.

Schizas N.V., Street G.T., Coull B.C., Chandler G.T., Quattro J.M. (1997) An efficient DNA extraction method for small metazoans. *Molecular marine biology and biotechnology*, **6**, 381–383.

Svensen C., Kiørboe T. (2000) Remote prey detection in *Oithona similis*: hydromechanical verses chemical cues. *Journal of Plankton Research*, **22**, 1155–1166.

Van Dover C.L., Reynolds G.T., Chave A.D., Tyson J.A. (1996) Light at deep-sea hydrothermal vents. *Geophysical Research Letters*, **23**, 2049–2052.

Van Dover C.L., Smith C.R., Ardron J., Arnaud S., Beaudoin Y., Bezaury J., Boland G., Billett D., Carr M., Cherkashov G. *et al.* (2011) Environmental Management of Deep-Sea Chemosynthetic Ecosystems: Justification of and Considerations for a Spatially Based Approach. Workshop 31 May-4 June 2010, Dinard, France. International Seabed Authority (ISA) Technical Study No. 9.

Van Gaest A.L. (2006) Ecology and early life history of *Bathynerita naticoidea*: Evidence for long-distance larval dispersal of a cold seep gastropod. M.S. Thesis, University of Oregon.

Visser A.W., Kiørboe T. (2006) Plankton motility patterns and encounter rates. *Oecologia*, **148**, 538–546.

Young C.M. (1995) Behavior and locomotion during the dispersal phase of larval life. In: McEdward L. (Ed.), *Ecology of Marine Larvae*. CRC Press, New York: 249–278.

Supporting Information

Additional Supporting Information may be found in the online version of this article:

File S1. A MATLAB (The Mathworks, Inc.) script, larval_tracking.m, to track a single larva in a video.

File S2. A MATLAB (The Mathworks, Inc.) script, reconstruct_3D.m, that uses the output of larval_tracking.m to reconstruct a 3D swimming trajectory.

File S3. Empirical test of new method for three-dimensional reconstruction of larval swimming trajectories.

Appendix 1

3D reconstruction method for ellipsoid

We approximated the morphology of the deep-sea polychaete larvae (and the shallow water larva in the empirical test) as a prolate spheroid with semi-principal axes a, b and c, where $a > b = c$. Below we provide a theoretical framework for 3D reconstruction for any ellipsoid. The orientation of a known ellipsoid can be found by measuring the length (L) and width (W) of its 2D projection. For a co-ordinate system where the x-axis passes through the long axis of the 2D projection, the z-axis lies perpendicular to the x-axis in the plane of the projection, and the y-axis is the unseen direction into or out of the pro-

jection (Fig. 3B). Note that this xyz co-ordinate system is a body fixed frame that moves as the larva moves, and is different from the spatially fixed xyz co-ordinate system used to describe the larva's motion. Spherical co-ordinates of the ellipsoid for this axis system are given by the polar angle from the z-axis, θ, and the azimuthal angle around the z-axis in the xy-plane, φ. The ellipsoid has semi-principal axes a, b and c, where $a > b \geq c$, corresponding to the axes described above. As the x-axis is fixed along one of the principal axes of the ellipsoid there are only two degrees of freedom for rotation of the ellipsoid: angle of rotation about the z-axis, γ (*i.e.* turning the z-axis creates the angular displacement, γ, between the original x-axis position and the new x-axis position), and the angle of rotation about the x-axis, ψ. θ and φ are used to identify positions on the ellipsoid surface relative to its internal axes, and γ and ψ are angles of rotation in space; γ is in reference to the vertical axis of the measurement system and ψ around the long axis of the ellipsoid.

For a non-rotated ellipsoid the Cartesian co-ordinates of the ellipsoid are given by equations (6–8):

$$x = a\cos\phi\sin\theta \tag{6}$$

$$z = b\sin\phi\sin\theta \tag{7}$$

$$y = c\cos\theta \tag{8}$$

Applying a general rotation of γ around the z-axis and a rotation of ψ around the x-axis transforms the Cartesian co-ordinates to equations (9) and (10). As we are only concerned with the projection of the ellipsoid onto the xz-plane, y is ignored from here on.

$$x = a\cos\gamma\cos\phi\sin\theta + c\cos\psi\cos\theta\sin\gamma + b\sin\psi\sin\gamma\sin\phi\sin\theta \tag{9}$$

$$z = b\cos\psi\sin\phi\sin\theta - c\cos\theta\sin\psi \tag{10}$$

For a non-rotated ellipsoid, the widest part of the xz ellipse projection will always lie at x = 0 so when finding ψ, φ is set to 90° and we are only concerned with z. To find the θ value at which the maximum z-value lies, the derivative of z [equation (10)] is taken with respect to θ and set equal to zero giving the elevation angle, θ_0, at which z is at a maximum [equation (11)].

$$\theta_0(\psi) = \cot^{-1}\left(-\frac{c}{b}\tan\psi\right) \tag{11}$$

As the xz ellipse is symmetric around the x-axis, the total width of the xz-projection is twice z evaluated at θ_0 [equation (10)], defined as width, W, in equation (12):

$$W(\psi) = 2b\cos\psi\sin[\theta_0(\psi)] - 2c\cos[\theta_0(\psi)]\sin\psi \tag{12}$$

There is no analytical solution to equation (12) for ψ, but numerical methods can be used to get a very accurate approximation of the angle of rotation as a function of xz-projection width, denoted by ψ (W).

A similar method is used to find the angle of inclination (γ) of the ellipsoid. The longest part of the ellipsoid will lie at z = 0 so θ is set to 90° and we are only concerned with x [equation (9)]. This time, the derivative of x is taken with respect to φ and set to zero to find the azimuthal angle, φ_o, at which x is at a maximum [equation (13)].

$$\phi_0(\gamma, W) = \tan^{-1}\left(\frac{b}{a}\sin[\psi(W)]\tan\gamma\right) \tag{13}$$

As the xz ellipse is symmetric around the z-axis the total length of the xz-projection is twice x evaluated at φ_o [equation (9)], defined as length, L, in equation (14):

$$L(\gamma, W) = 2a\cos\gamma\cos[\phi_0(\gamma, W)] + 2b\sin[\psi(W)]\sin\gamma\sin[\phi_0(\gamma, W)] \tag{14}$$

Equation (14) can be solved numerically to get the angle of inclination (γ) into the page, γ(L,W), as a function of xz-projection length and width.